Institute of Space and Aeronautical Science, University of Tokyo
Report No. 508, March 1974

A High Precision Experiment on the Buckling of Spherical Caps Subjected to External Pressure

By

Megumi SUNAKAWA and Kazuo ICHIDA

Summary: A high precision experiment has been extensively carried out to bridge the gap between the theoretical and experimental buckling loads of spherical caps subjected to external pressure. The details of the forming process of test specimens, experimental arrangements and procedures, and reliable data on the buckling load as well as the deflection and strain distributions obtained are reported. It is shown that the buckling load of perfect spherical caps is close to the so-called classical value, the pre- and postbuckling deformation patterns are axisymmetrical, prebuckling deformation patterns are not fixed but change through the loading and are subject to the geometrical parameter, the number of waves in the meridional direction increases and the so-called boundary layer is formed as the geometrical parameter becomes larger, the membrane state of strains is predominant and load vs. deflection curves are almost linear for large values of the geometrical parameter in the prebuckling state of equilibrium, the deflection of shells is small up to the occurrence of buckling, and hence the small deflection theory will play still an important role in analyzing the stability of spherical caps subjected to external pressure. The detailed discussion on the results seems to contribute to make the mechanism of the buckling of spherical shells clear.

NOMENCLATURE

a	horizontal radius of spherical cap
h	shell thickness
n	number of half-waves of deflection in the meridional direction
p	external pressure load
$p_{cl} \equiv 2[3(1-\nu^2)]^{-1/2}E(h/R)^2$	classical buckling pressure for the complete sphere
p_{cr}	experimental buckling pressure
$q \equiv p/p_{cl}$	nondimensional load
$q_{cr} \equiv p_{cr}/p_{cl}$	nondimensional buckling load
$q_1 \equiv p/p_{cr}$	nondimensional load
r	horizontal coordinate of a point in the shell
E	Young's modulus
H	rise of sherical cap
R	radius of curvature of spherical shell
β_0	reference semi-apex angle
δ	deflection of shell in the R-direction

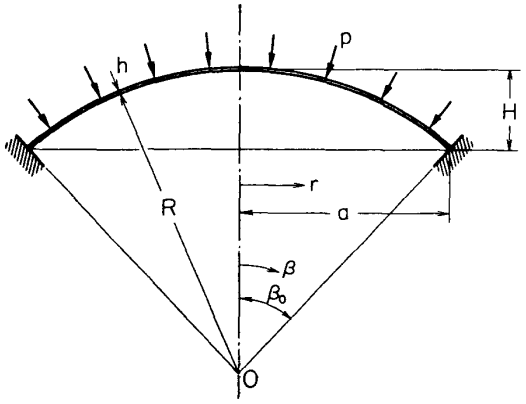

FIG. 1. Sherical cap.

$\bar{\delta} \equiv \delta/h$	nondimensional deflection
$\bar{\delta}_a \equiv \delta_{\max}/h$	nondimensional maximum deflection
$\bar{\delta}_c \equiv \delta_c/h$	nondimensional deflection at the center
$\varepsilon_0, \varepsilon_b$	in-plane and bending strains, respectively; the second subscript "r" or "θ" shows the median or circumferential component
ν	Poisson's ratio
$\lambda \equiv 2[3(1-\nu^2)]^{1/4}(H/h)^{1/2}$	geometrical parameter for spherical caps
$\phi \equiv \beta_0^2(R/h)$	geometrical parameter for spherical caps
$\xi \equiv r/a$	nondimensional horizontal coordinate

1. INTRODUCTION

The problems of the stability of spherical shells subjected to external pressure and of cylindrical shells under axial load are the typical imperfection-sensitive ones. Therefore, many investigations [*1*] have been carried out so far to make the true nature of large discrepancy existed between the theoretical and experimental buckling loads clear.

Theoretical buckling pressures of perfect spherical caps have been settled down into the following two values. One is the so-called upper buckling value [*2*] as the symmetrical deformation, and the other is the bifurcation value [*3*] as the unsymmetrical one, while experimental values have been scattered far and wide [*4*]~[*6*]. The history of the research on the subject matter has been reviewed critically by one of the present authors [*1*] and is not duplicated herein.

To bridge the gap mentioned above a high precision experiment has been carried out in detail and with great care at the authors' laboratory.

In the present paper, the forming process of test specimens, experimental arrangements and procedures, and the buckling load as well as the deflection and strain distributions obtained in the experiment are reported.

It is quite difficult, especially for instability problems of shells, to carry out experiments whose conditions are consistent completely with assumptions and approximations made in theoretical analyses. But, the authors' opinion that ex-

perimental values have to coincide with theoretical ones when conditions in both cases are the same is now being demonstrated.

The present work forms a link in the chain of the authors' research which intends to make the mechanism of instability phenomena in shells clear.

2. Experimental Arrangements and Procedures

2.1. Forming of Specimen

It is essentially important to carry out the experiment on perfect shells, and so the greatest care was paid in forming test specimens.

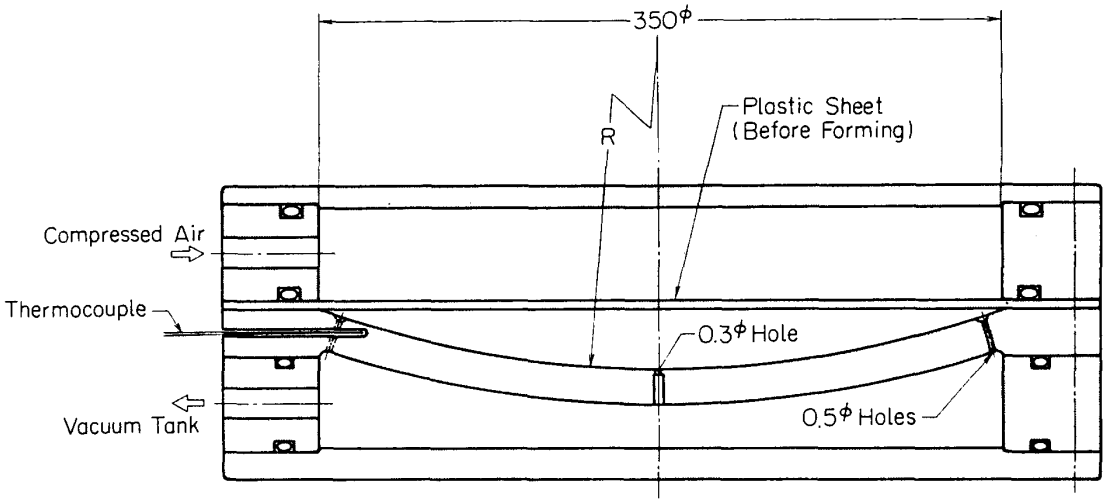

Fig. 2. Mold used in forming.

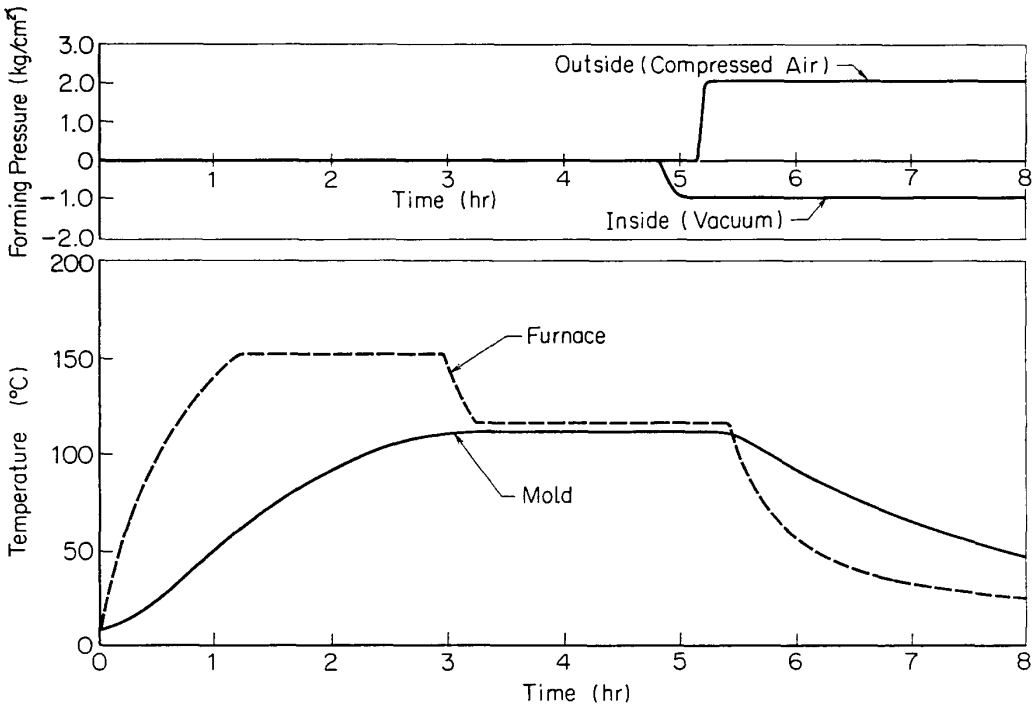

Fig. 3. An example of forming procedure.

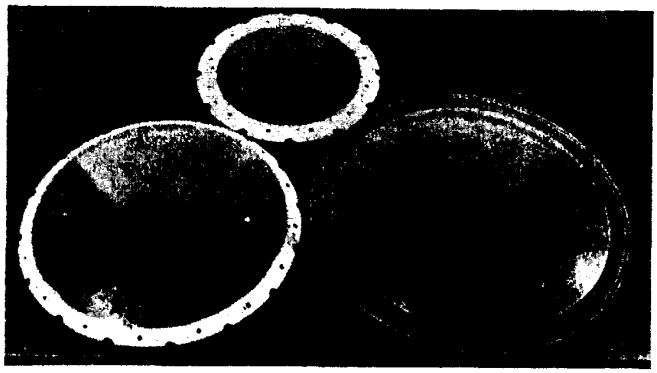

FIG. 4. Formed spherical caps.

TABLE 1. Geometry of test specimens.

Radius of curvature (mm)	R	300, 400, 500, 750, 1000, 1500
Thickness (mm)	h	0.5~3.0
Radius to thickness ratio	R/h	100~3000
Base radius (mm)	a	100, 150
Semi-apex angle (rad.)	β_0	0.067, 0.10, 0.13, 0.15, 0.20, 0.25, 0.31, 0.34, 0.38, 0.52
Geometrical parameter	λ	2.64~22.5
Geometrical parameter	ϕ	2.20~160

TABLE 2. Number of test specimens, N.

$2a$ (mm)	R (mm)	h (mm)	N	λ
200	1,500	1.77	1	3.43
	1,000	1.00~3.07	14	3.22~ 5.64
	750	0.51~3.07	15	3.73~ 8.79
	500	0.53~1.79	6	5.96~11.0
300	1,500	1.84~3.15	3	3.88~ 5.09
	1,000	1.01~2.98	13	4.91~ 8.31
	750	0.51~2.41	30	6.27~13.6
	500	0.51~2.49	34	7.65~17.0
	400	0.73~1.85	21	9.95~15.9
	300	0.56~1.54	27	12.6 ~21.3

There are several common processes to form shell specimens: namely, spinning process, air vacuum forming process, hydro-forming process, machining process, electro-plating process, and explosive forming process.

After the detailed examination of the above-mentioned and another processes, the authors decided to form flat PMMA (Poly Methyl Methacrylate) plates into

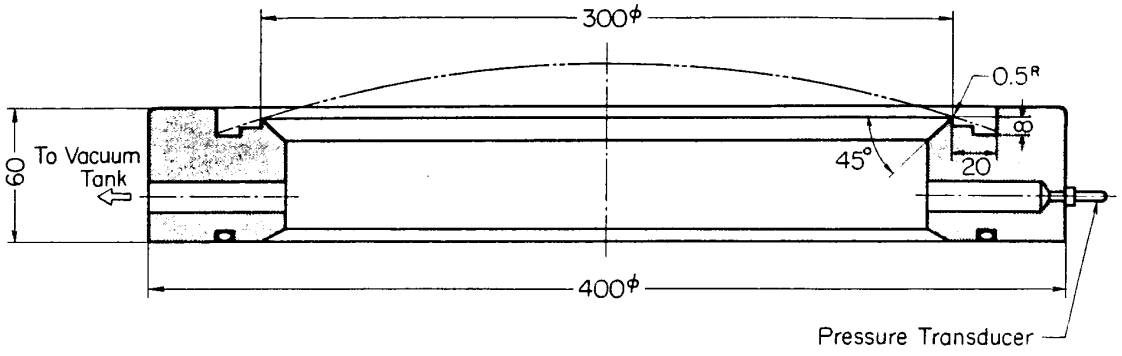

FIG. 5. Edge supporting ring.

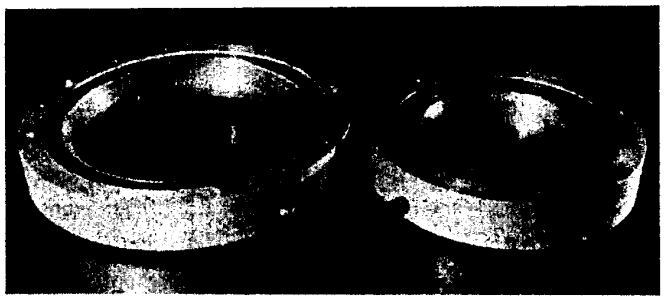

FIG. 6. Test specimens bonded to supporting rings.

spherical caps by the use of the air vacuum forming process at elevated temperature. In the forming of test specimen, a PMMA plate set on a mold is placed in an furnace at a temperature ranging 105~115°C and the air trapped in the gap between the plate and the mold is evacuated gradually and carefully until the plate fits perfectly to the spherical surface of the mold. The process adopted by the authors has been discussed in detail in Ref. 7. The mold used in the forming, an example of forming prcoedure, and spherical caps formed are shown in Figs. 2, 3 and 4, respectively. There found little initial geometrical imperfections and residual stresses in specimens formed. The variation of the shell thickness was found within $\pm 1.5\%$ of the mean thickness, and so it can be considered that specimens are nearly perfect. The ranges of the radius of curvature, R, the shell thickness, h, and the geometrical parameter, λ, of test specimens are 300~1500 mm, 0.5~3.0 mm, and 2.64~22.5, respectively. The geometrical dimensions and number of specimens tested are listed in Tables 1 and 2, respectively.

The two geometrical parameters for shallow spherical caps, λ and ϕ are connected approximately with each other by the following relationships,

$$\lambda^2 \fallingdotseq 3.17\phi, \qquad (\nu=0.4),$$
$$\fallingdotseq 3.27\phi, \qquad (\nu=1/3).$$

Material constants are connected directly with the buckling load, and so Young's modulus of test specimens formed at elevated temperature was measured one by one. As a by-product of accurate measurements of strain and elastic modulus, a

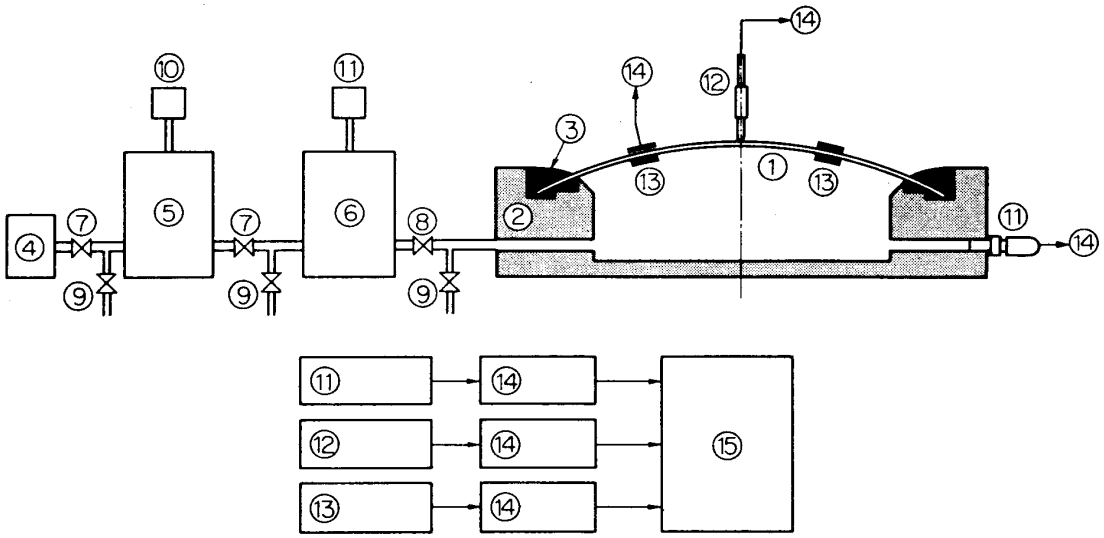

FIG. 7. Experiment set-up (schematic).

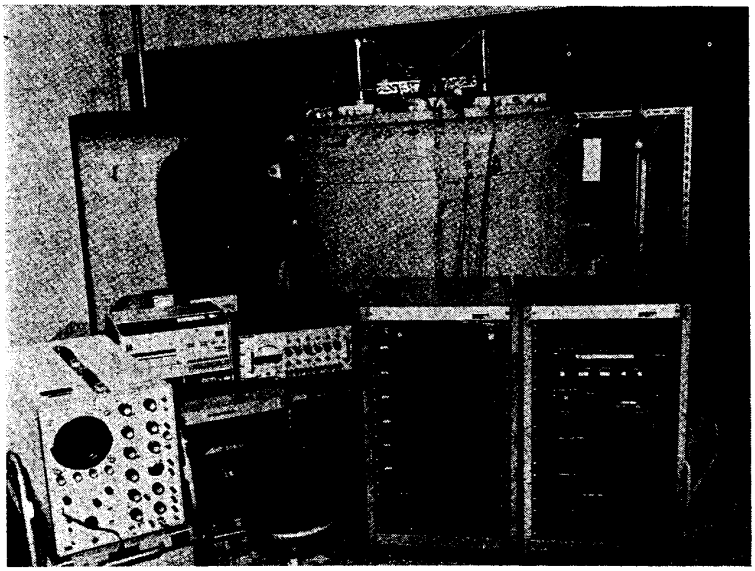

FIG. 8. Experimental arrangements.

comment on gauge factor of electric-resistance wire strain gauges has been reported [*16*].

2.2. Edge Support of Test Specimen

The edge support characterizing the rigidly clamped boundary conditions was

FIG. 9. Pressure transducer.

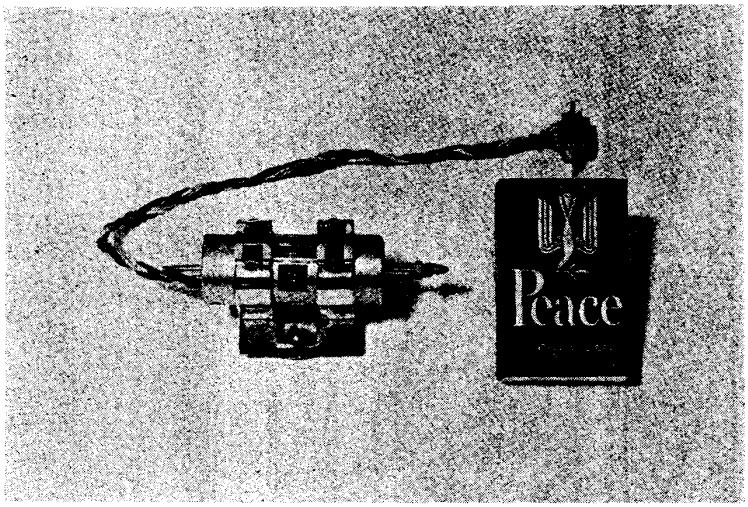

FIG. 10. Displacement transducer.

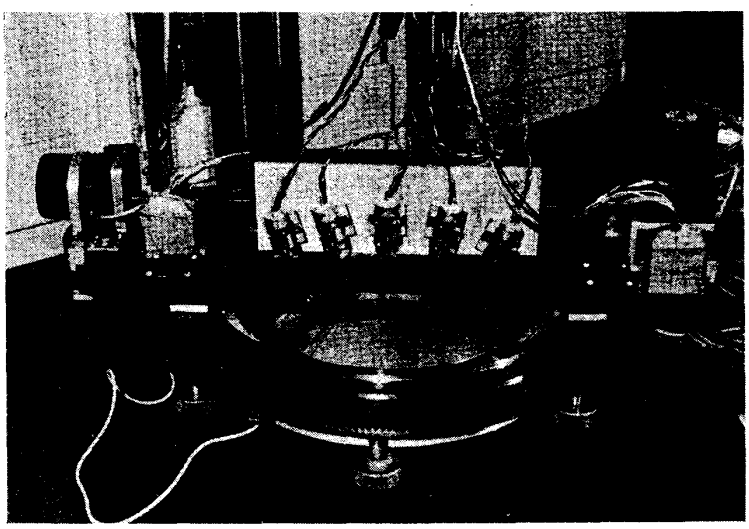

FIG. 11. Displacement scanner.

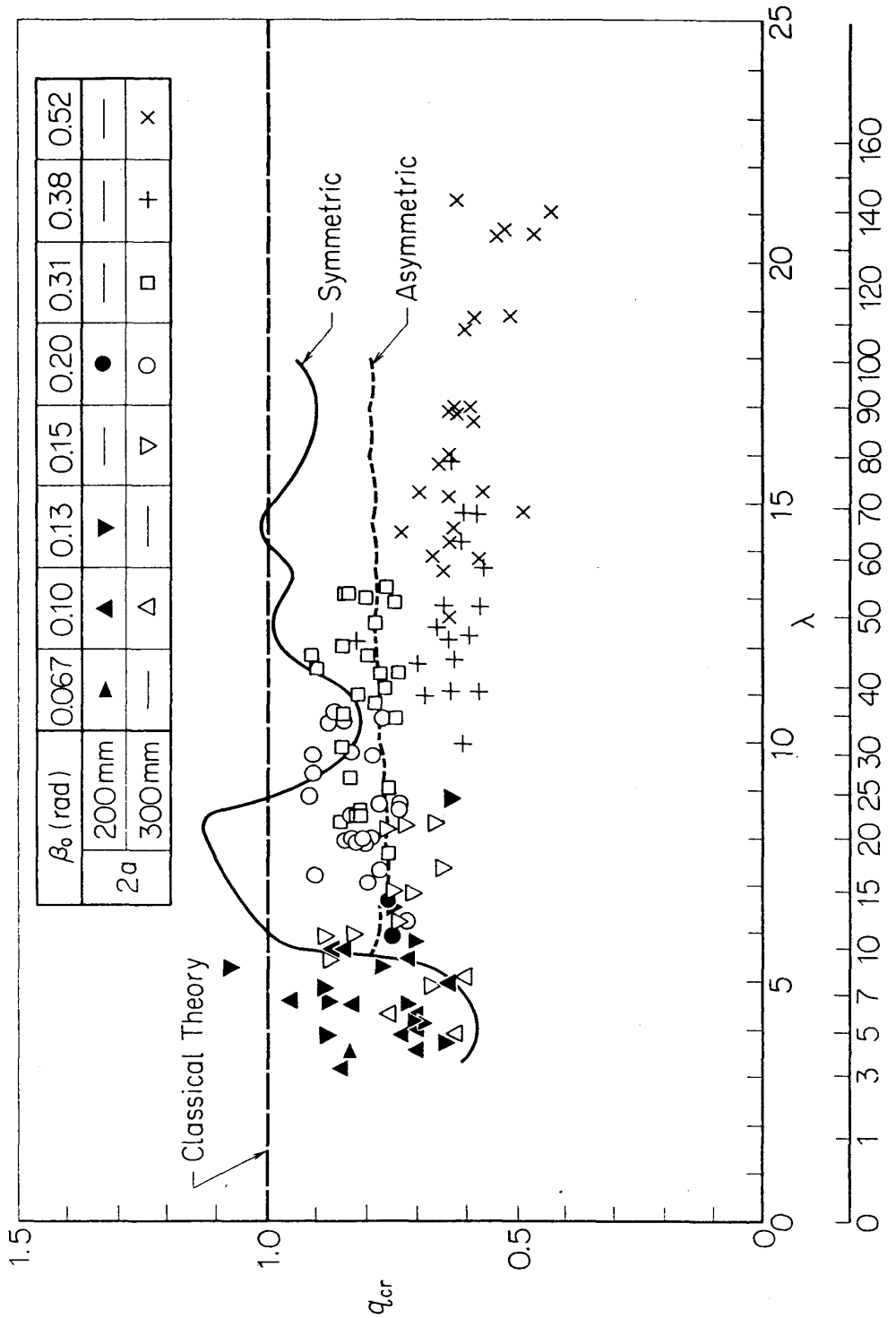

FIG. 12. Variation of buckling load with geometrical parameter.

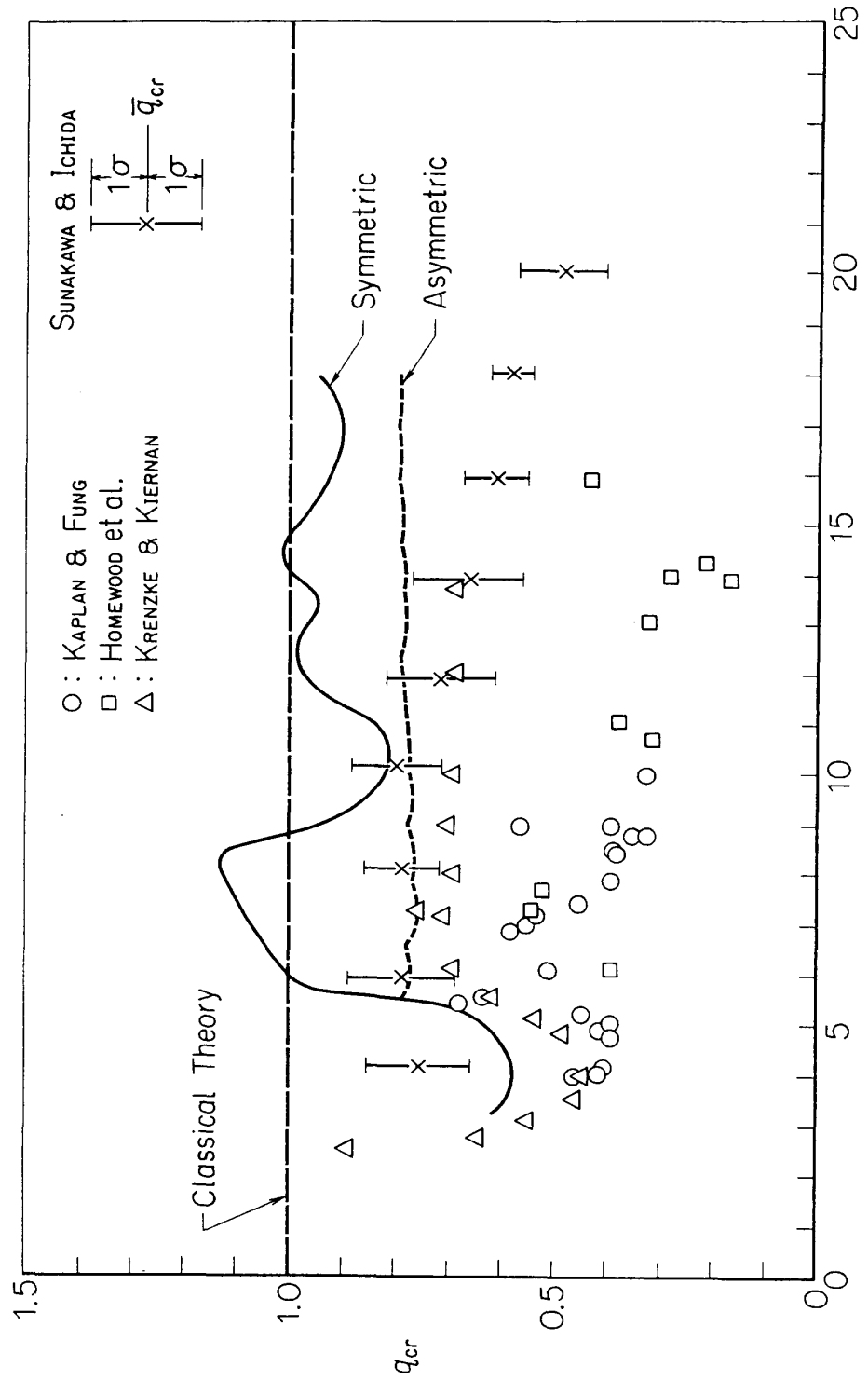

FIG. 13. Mean and variance of data in segments $\Delta\lambda=2$.

established by bonding the test specimen with an epoxy resin adhesive to the supporting ring.

Edge conditions as well as geometrical imperfections affect directly the prebuckling deformation, buckled pattern at the instant of its generation, and hence buckling load. Some endeavor to satisfy the clamped edge conditions was made which has been reported in some detail in Ref. 7. A edge supporting ring and bonded specimens are shown in Figs. 5 and 6, respectively.

2.3. *Experiment*

The experimental set-up (Figs. 7 and 8) consists of a test specimen, a support ring, a vacuum pump, a vacuum tank, a loading tank, regulating valves, manometers, pressure transducers (Fig. 9), displacement and strain transducers, amplifiers and recorders. Displacement transducers of a differential-transformer type (Fig. 10) are installed on a specially designed displacement pick-up device (Fig. 11), so that the displacement over the entire surface of the test specimen can be measured.

All apparatuses used in the experiment had been calibrated repeatedly under the on-line condition and sustained efforts had been put on to obtain reliable data by carrying out the experiment precisely.

After setting up the test specimen and all pick-up devices, the air inside the specimen is evacuated gradually and so the external pressure load is applied quasi-statically on the specimen. At the same time, the magnitudes of load, deflection and strain are recorded continuously. The load is held constant when necessary, and detailed distributions of deflection and strain are measured. The above-mentioned measurements are carried out until the buckling occurs, and phenomena of snapping back are also checked for some cases.

The measurement had been repeated and the same results were obtained at every corresponding run.

In the following sections, the experimental results are presented and discussed.

3. Buckling Load

In Fig. 12, the buckling load, q_{cr}, is plotted against the geometrical parameter, λ, where E_0 and ν have been put as $E_0=300$ kg/mm^2 (20°C) and $\nu=0.4$. E_0 means the static modulus of elasticity when the material property of PMMA is approximated by a three-element model [*17*], that is, $E_0=1/(1/E_1+1/E_2)$. The experimental data are then grouped within the segment of $\Delta\lambda=2$, and the mean, $\bar{q}_{cr}$, and the variance, σ^2, are evaluated within each segment (Fig. 13). Some of theoretical and experimental results [*2*$\sim$*6*] reported so far are also shown in these figures.

The results indicate that the experimental buckling load does not necessarily coincide with those obtained by theoretical analyses but is very close to the classical buckling pressure for the complete spherical shell. The buckling load decreases slightly as the value of the geometrical parameter increases beyond $\lambda\fallingdotseq 13$. The plot shows that there exists no minimal point around $\lambda=4$ in the buckling load

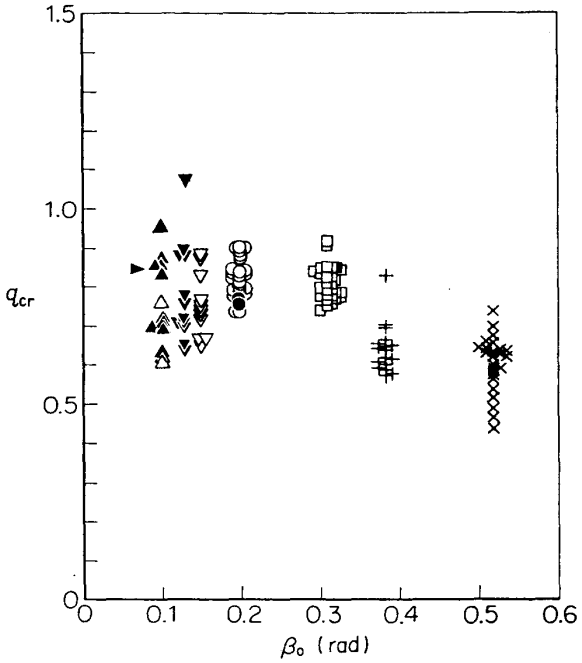

FIG. 14. Variation of q_{cr} with β_0.

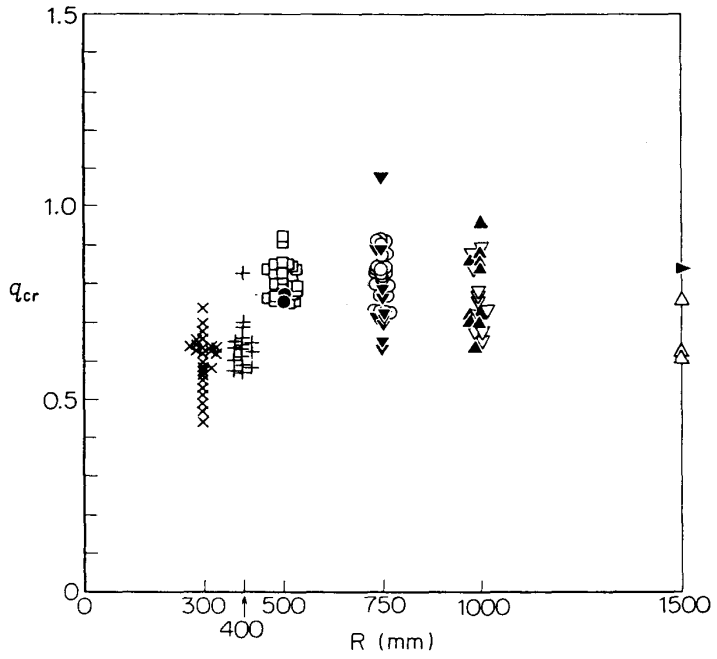

FIG. 15. Variation of q_{cr} with R.

vs. geometrical parameter curve as predicted by nonlinear theoretical analyses. The shells exhibit no unstable phenomena where geometrical parameter is smaller than about 3.25, which agrees with previous results.

Variations of the buckling load, q_{cr}, with the semi-apex angle, β_0, radius of curvature, R, wall-thickness, h, and ratio of radius of curvature to wall-thickness, R/h, are shown in Fig. 14 through Fig. 17 inclusive. It can be seen from Figs. 12

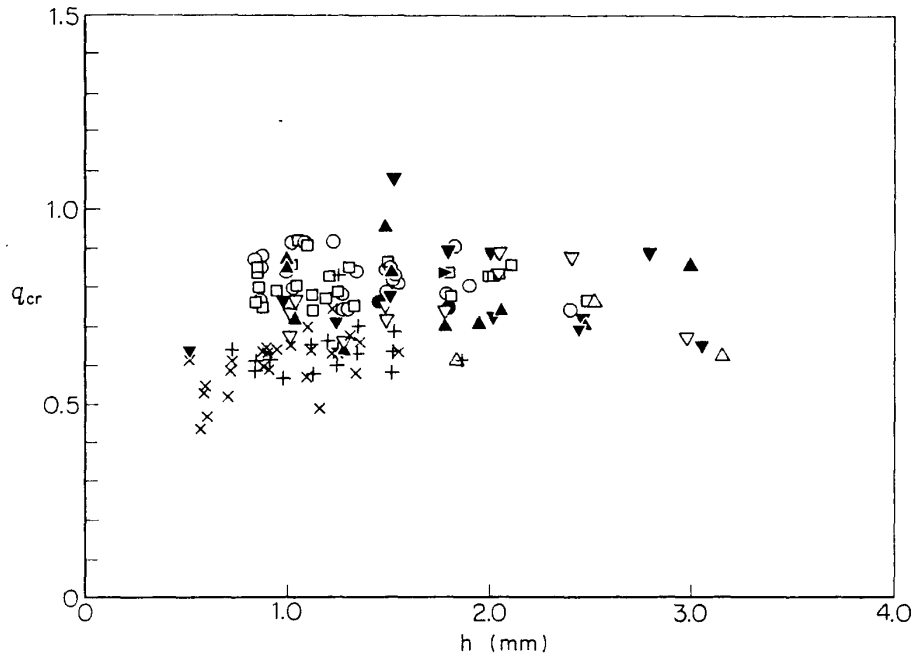

FIG. 16. Variation of q_{cr} with h.

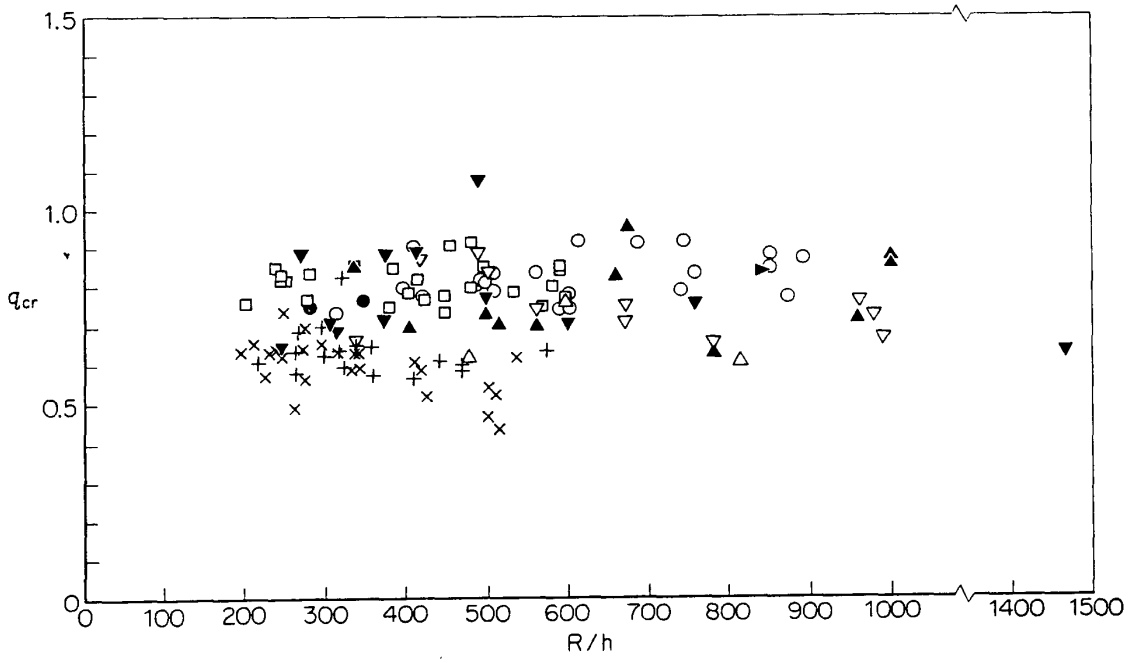

FIG. 17. Variation of q_{cr} with R/h.

and 14 that the experimental data have scattered in some degree for very small values of β_0 and that the buckling load becomes somewhat smaller for large values of β_0 whereas it is in doubt about the assumption that shells are shallow for $\beta_0=$ 0.38 and 0.52. Figures 16 and 17 show that changes in h and R/h have no marked effect on q_{cr}.

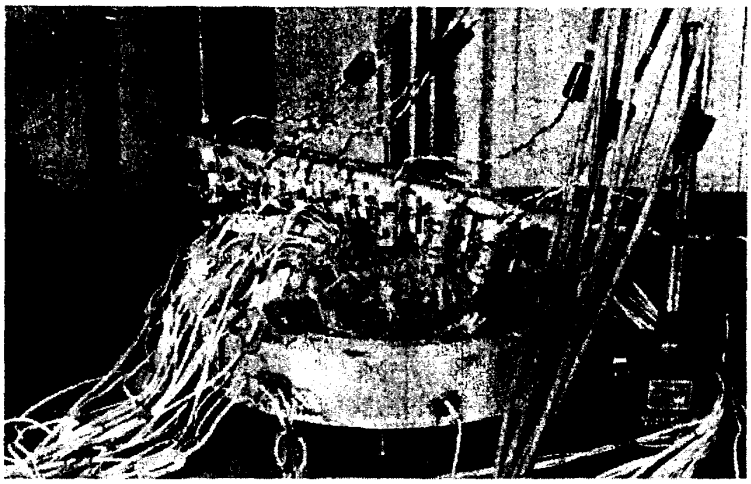

FIG. 18. An example of measurement of deflection and strain.

The experimental results do not prove the unsymmetrical buckling theory [3] as though they apparently do, and the fact has been made clear from the observation of buckling patterns by high speed movie pictures.

4. DEFLECTION PATTERN AND STRAIN DISTRIBUTION

4.1. Outline of Measurement

With a series of preliminary experiments by the use of displacement scanner mentioned in 2.3 and electric-resistance wire strain gauges, it had been confirmed that the deflection pattern of and strain distribution in shells are axisymmetrical with respect to the center. And so, locations of displacement transducers were fixed after the symmetricity of the deflection pattern was reconfirmed, and then changes in the deflection pattern and strain distribution with the external pressure were measured (Fig. 18). The radius of curvature of semispherical end of the displacement transducer is 2.3 mm and each measuring force is 8 gr. Strain gauges of 2 mm in gauge length were adhesive-bonded in the meridional and circumferential directions on both surfaces, and each strain is decomposed into the in-plane and bending components. The locations of displacement and strain transducers vary depending upon the value of geometrical parameter of test specimens and on account of the purpose of the every measurement (Fig. 18).

4.2. Prebuckling Deformation

The changes in the deflection on the outer surface, δ, and in in-plane strains, $\varepsilon_{0,r}$ and $\varepsilon_{0,\theta}$ and bending strains, $\varepsilon_{b,r}$ and $\varepsilon_{b,\theta}$ with the external pressure load, q_1, are shown in Figs. 19. Since it has been confirmed on the basis of observations made on more than one hundred of cases that deformations are axisymmetrical with respect to the center, the distributions of deflection and strain on a certain meridian only have been shown in these figures. Symbols in brackets following values of geometrical parameter are those given in Fig. 12.

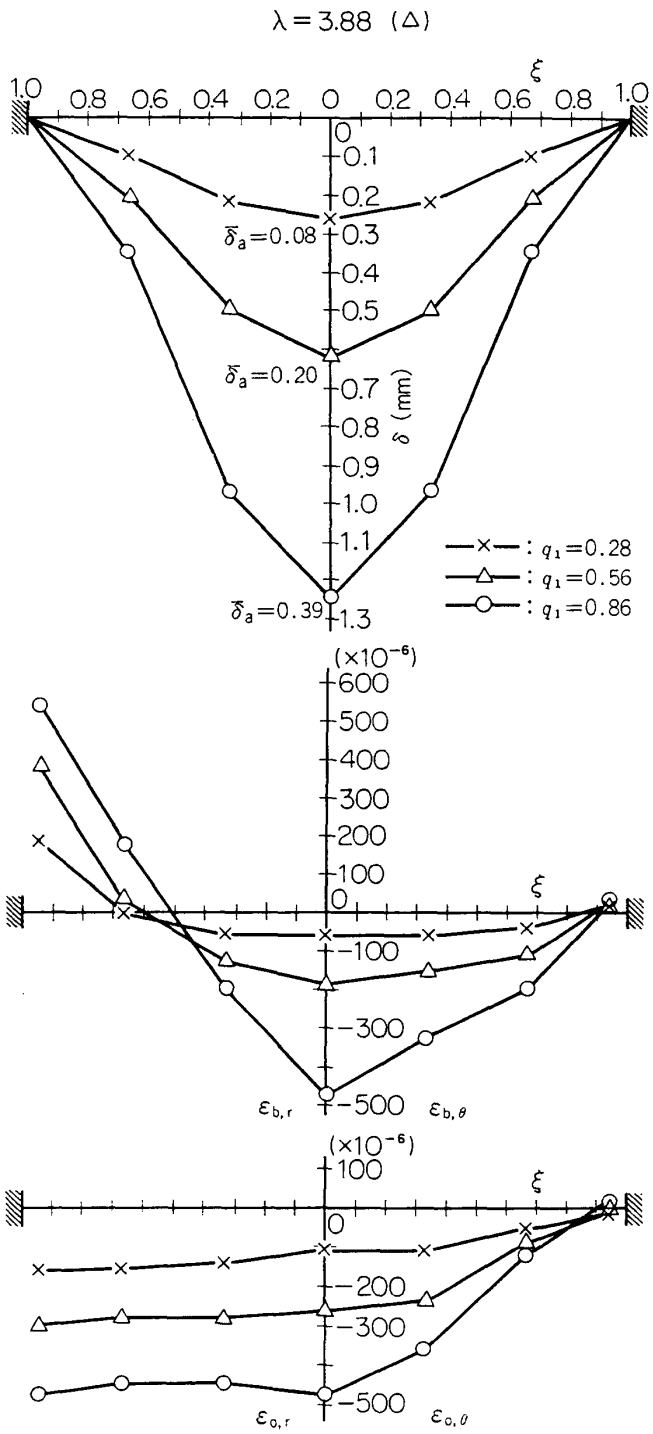

FIG. 19 (a). Deflection pattern and strain distribution.

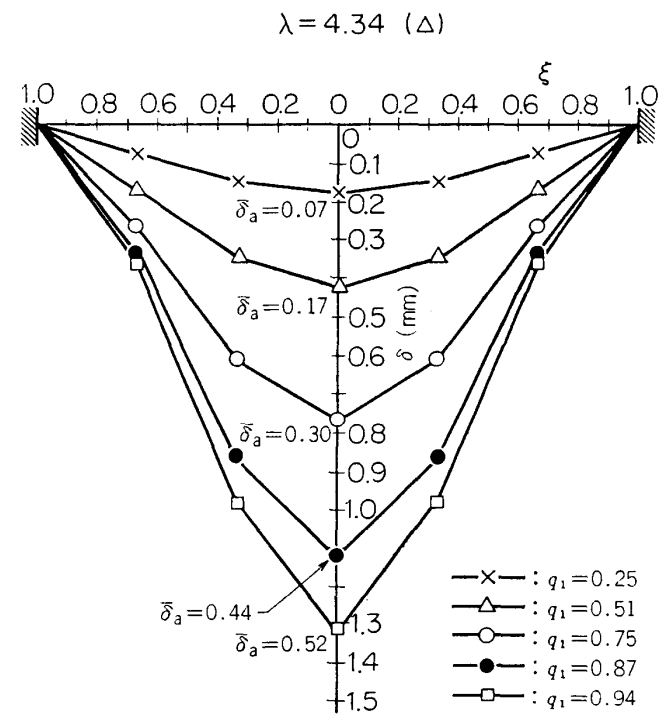

FIG. 19 (b)

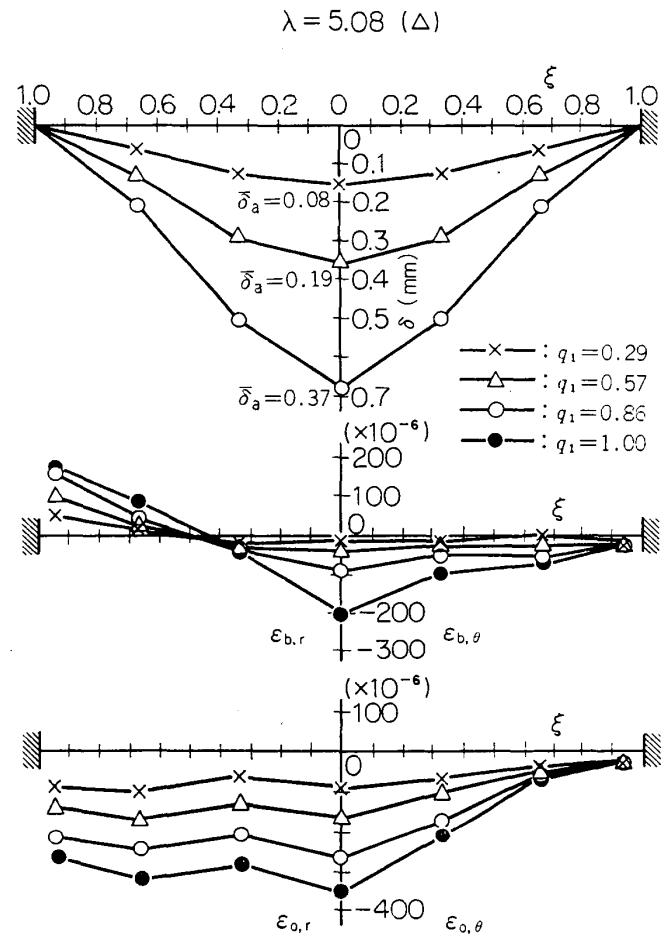

FIG. 19 (c)

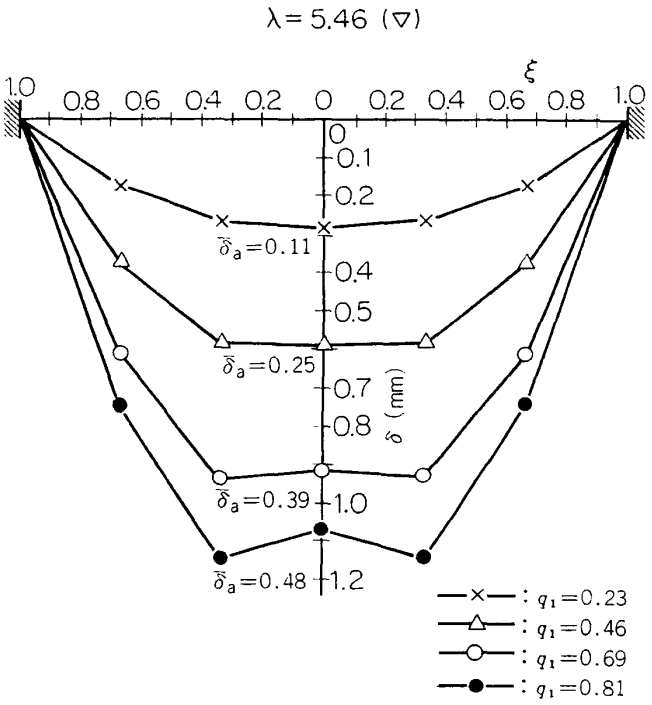

FIG. 19 (d)

It can be seen from these figures that prebuckling deflection patterns are not fixed but change with the loading and that the number of waves in the meridional direction increases with the increase of the value of geometrical parameter. It is observed, when the geometrical parameter becomes larger, that the deflection and strain increase markedly only in the vicinity of the clamped edge, that is, the so-called boundary layer develops, and they ripple outside the boundary layer.

The strains change almost linearly with the loading and in-plane components of strains are generally much larger than bending components. The variation of bending components of strains corresponds to the deflection pattern, while in-plane components are relatively uniform except around the boundary layer.

The predominant number of half-waves before buckling is shown in Fig. 20 as a function of geometrical parameter. It seems that values of n are related with not only λ but also β_0. Wave patterns are not necessarily the same even for the same values of n but different markedly depending on values of β_0. Only a few patterns of $n=3$ were observed in the experiment.

The variation of q_{cr} ($\bar{q}_{cr}$ and σ^2) with n is shown in Fig. 21. It can be seen from Fig. 21 that q_{cr} decreases as n increases, and there might be some another tendency between cases where n's are odd and even numbers.

Relationships between q_1 and $\bar{\delta}_a$ and between q_1 and $\bar{\delta}_c$ are shown in Figs. 22 and 23, respectively. Continuous changes in deflection at specified points on the shell surface were observed and are shown in Figs. 24. In Figs. 24, (a) is the case where no buckling occurs, (b) and (c) correspond to cases of $n=1$, (d) $n=2$, and (e) $n=7$. It might be understood from Figs. 24(b) and (c) that unstable postbuckling behaviors were traced, but it is not so and these results

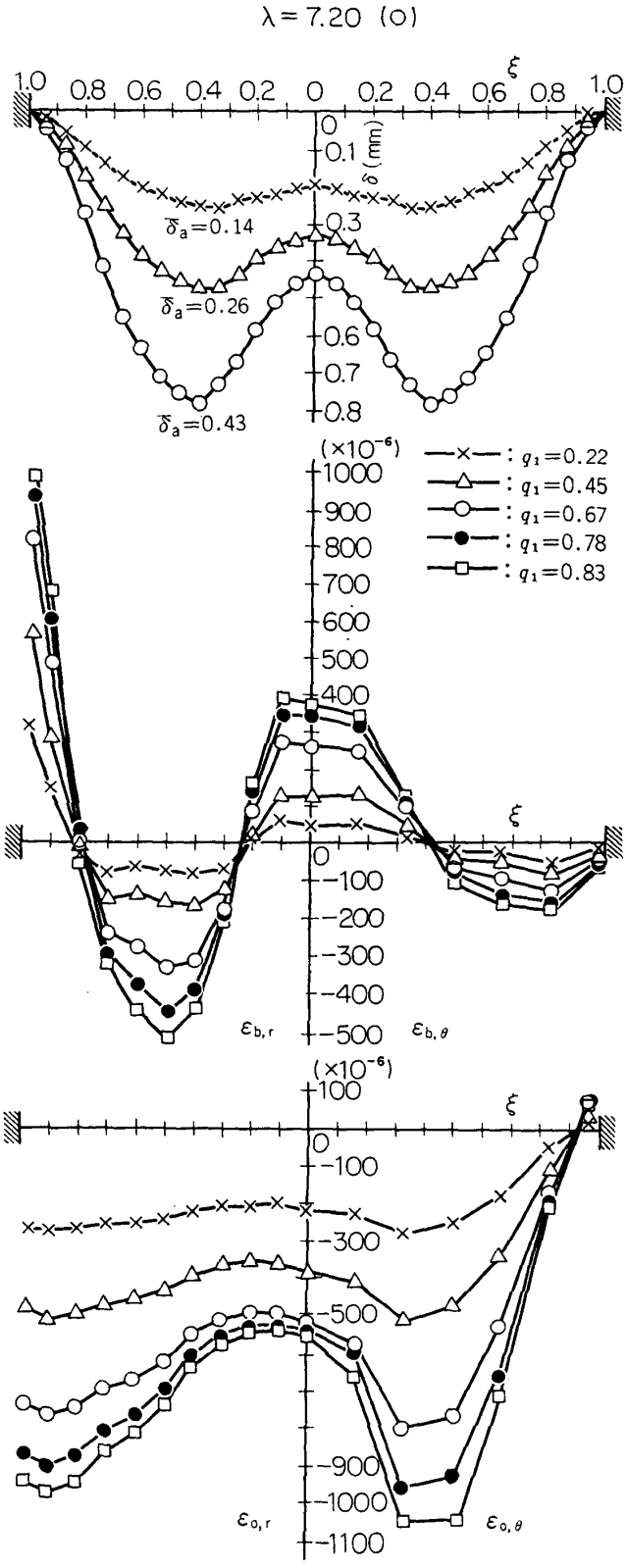

FIG. 19 (e)

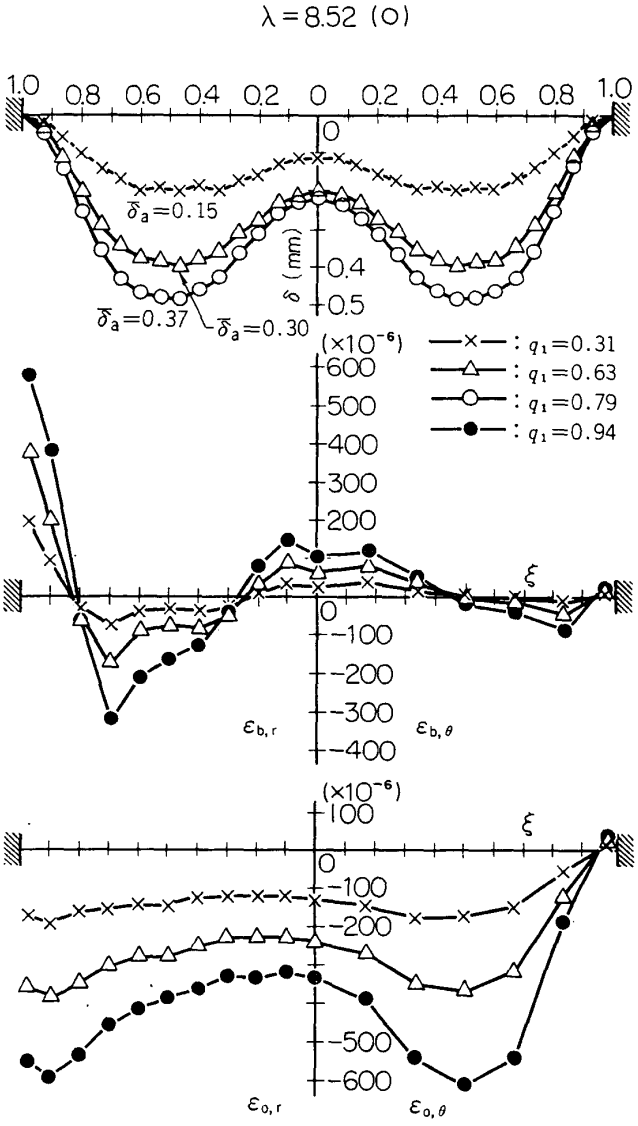

FIG. 19 (f)

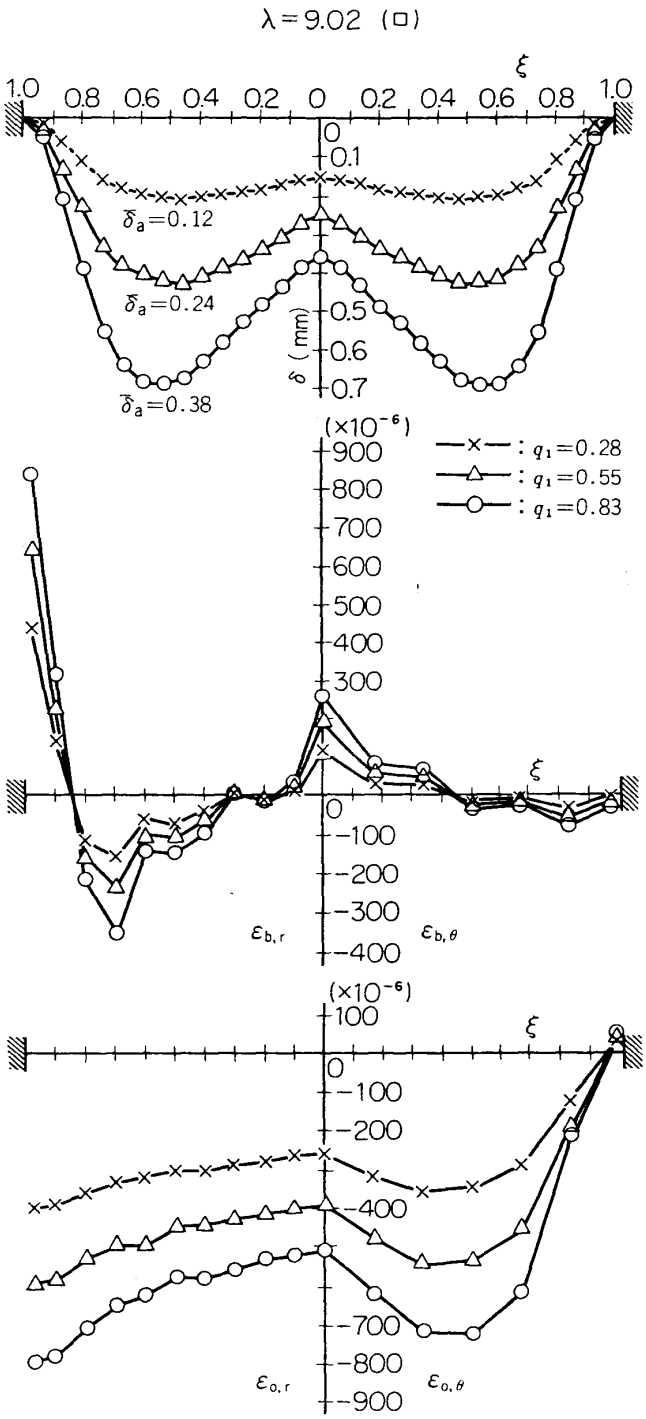

FIG. 19 (g)

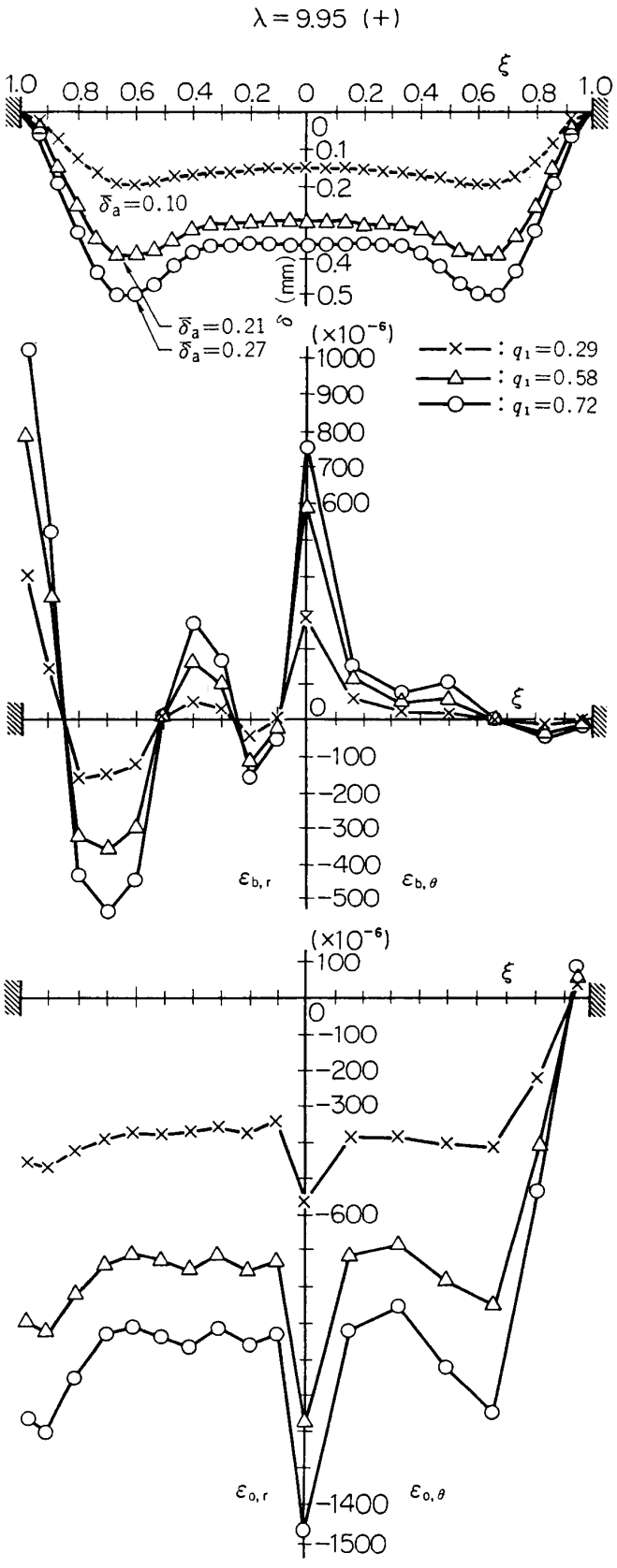

FIG. 19 (h)

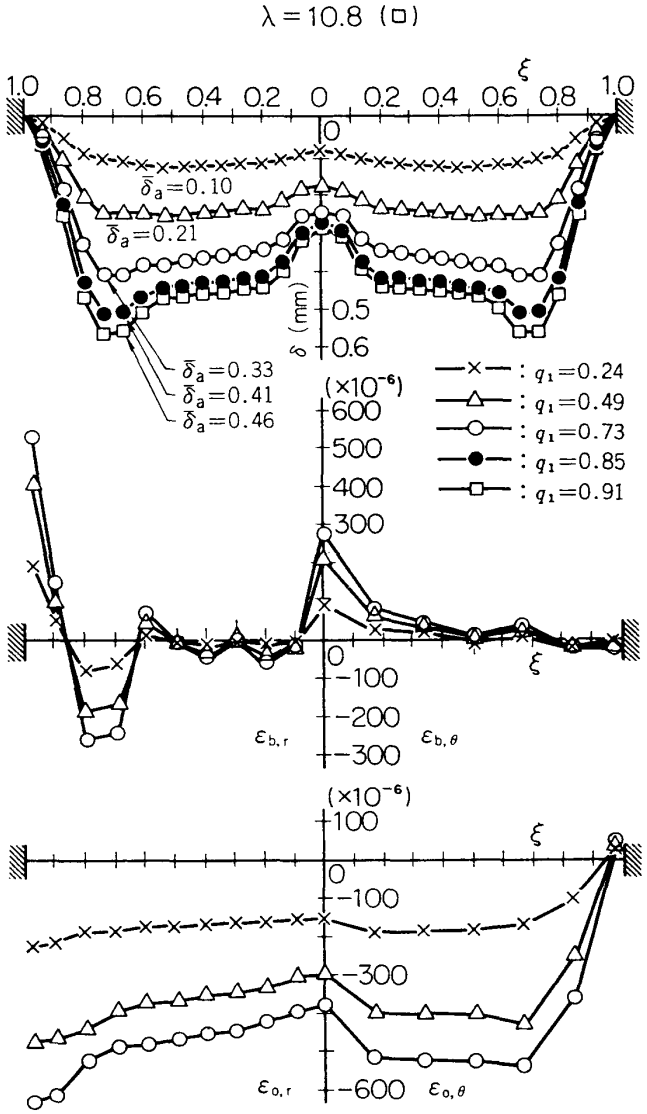

FIG. 19 (i)

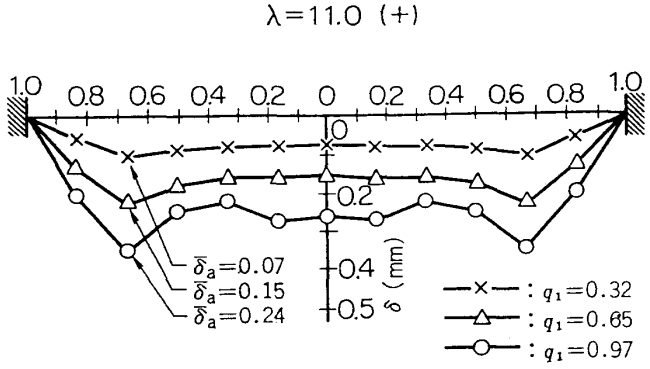

FIG. 19 (j)

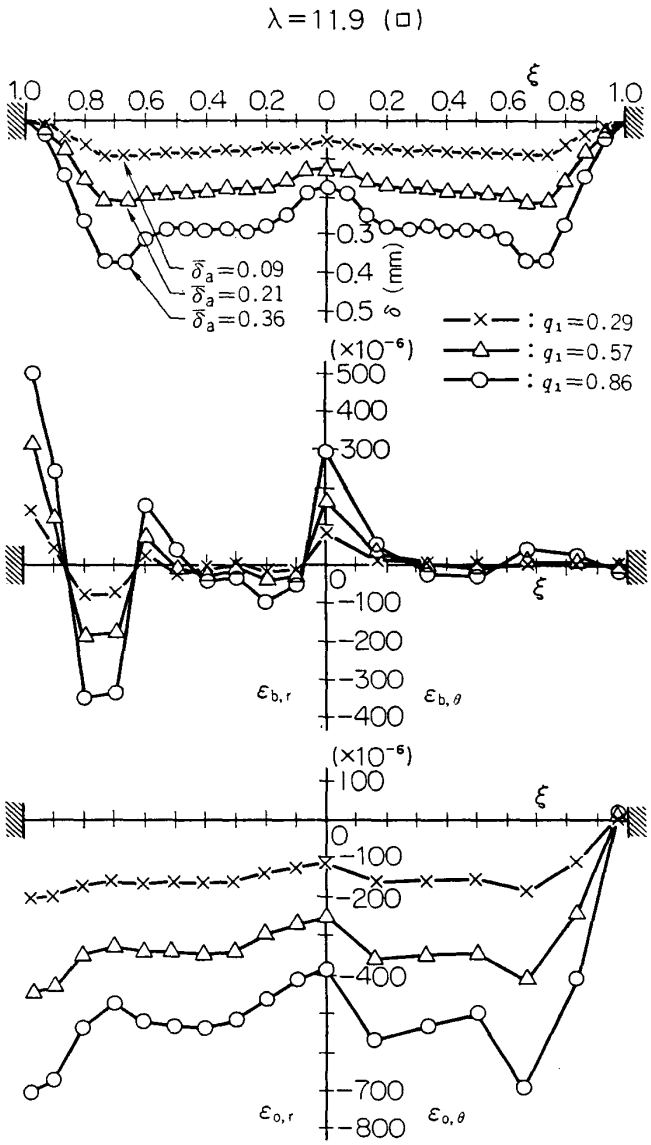

FIG. 19 (k)

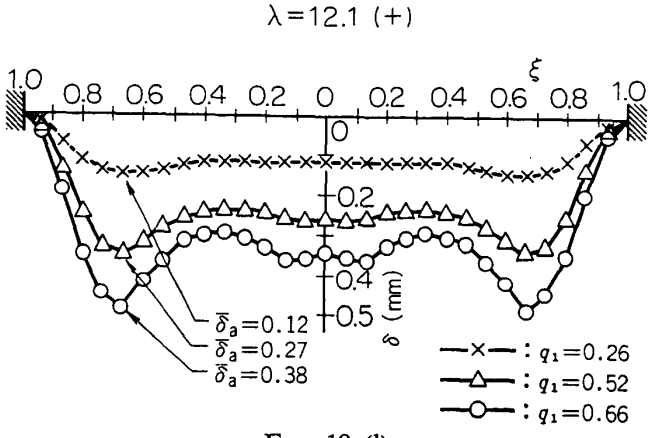

FIG. 19 (l)

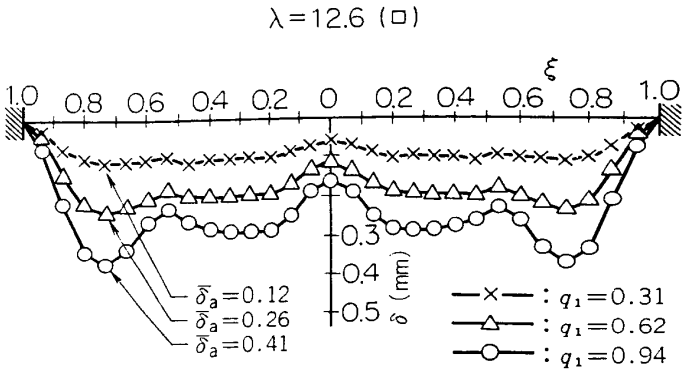

FIG. 19 (m)

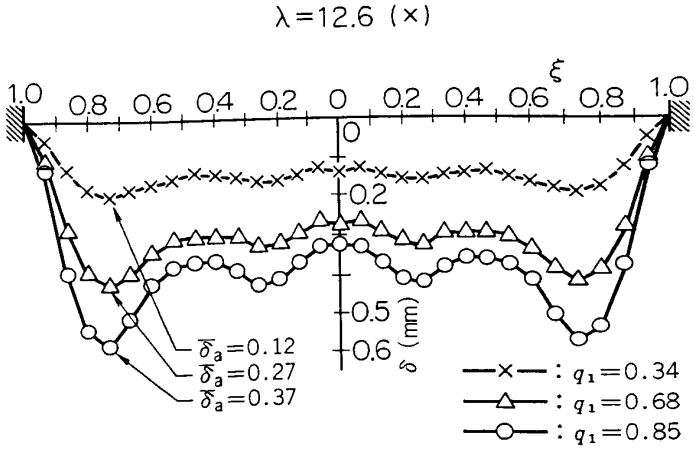

FIG. 19 (n)

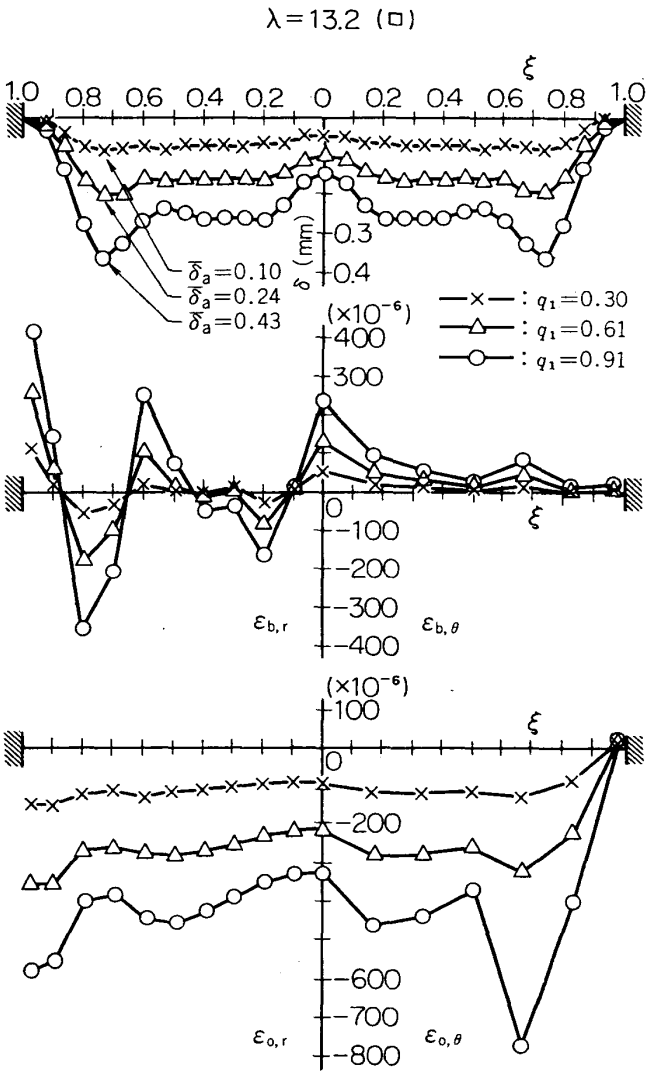

FIG. 19 (o)

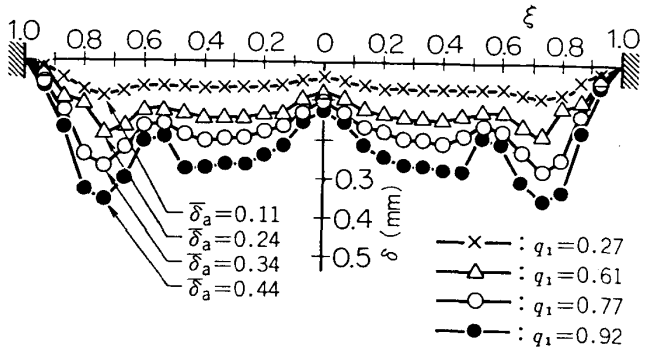

FIG. 19 (p)

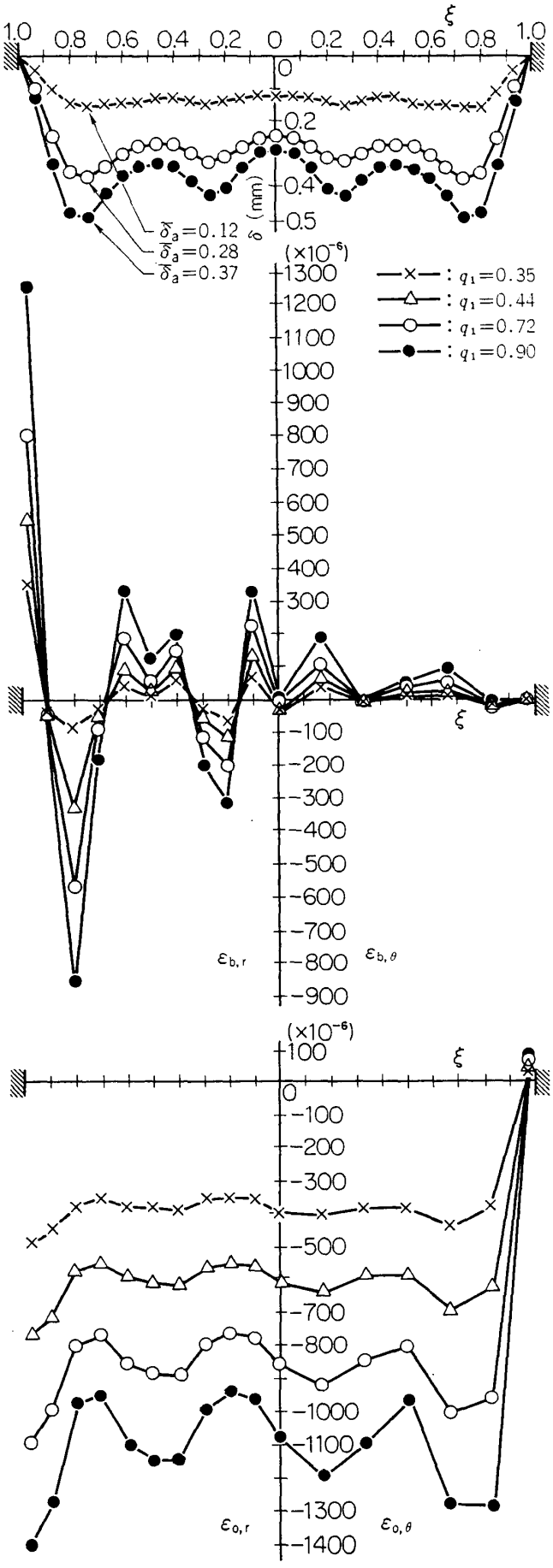

FIG. 19 (q)

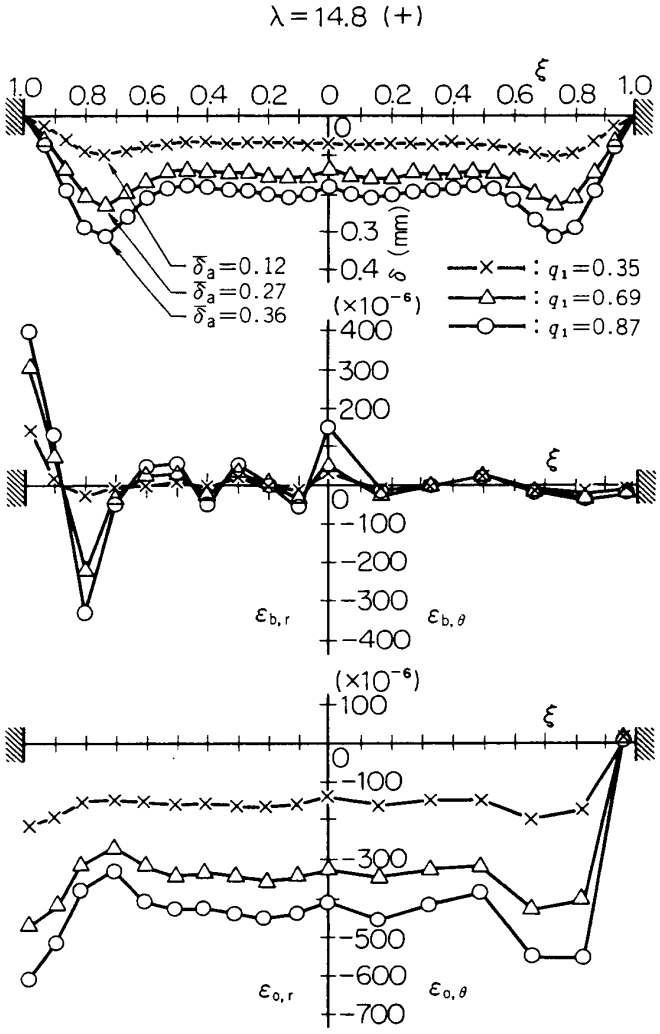

FIG. 19 (r)

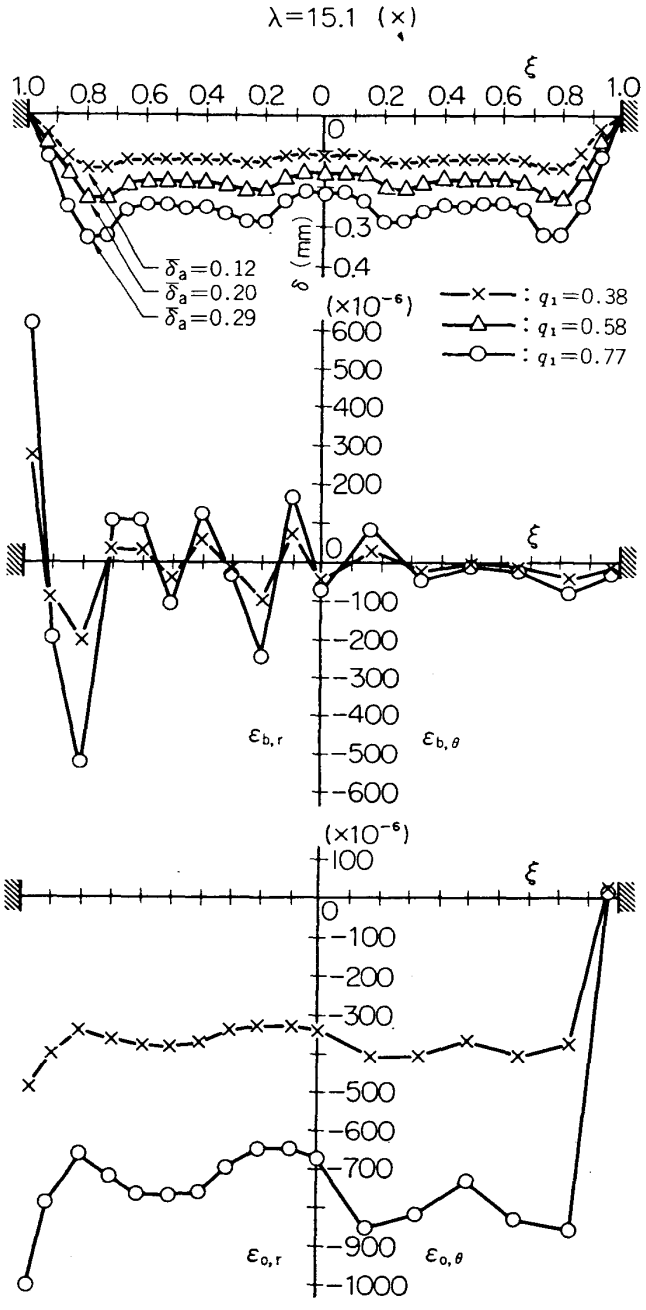

FIG. 19 (s)

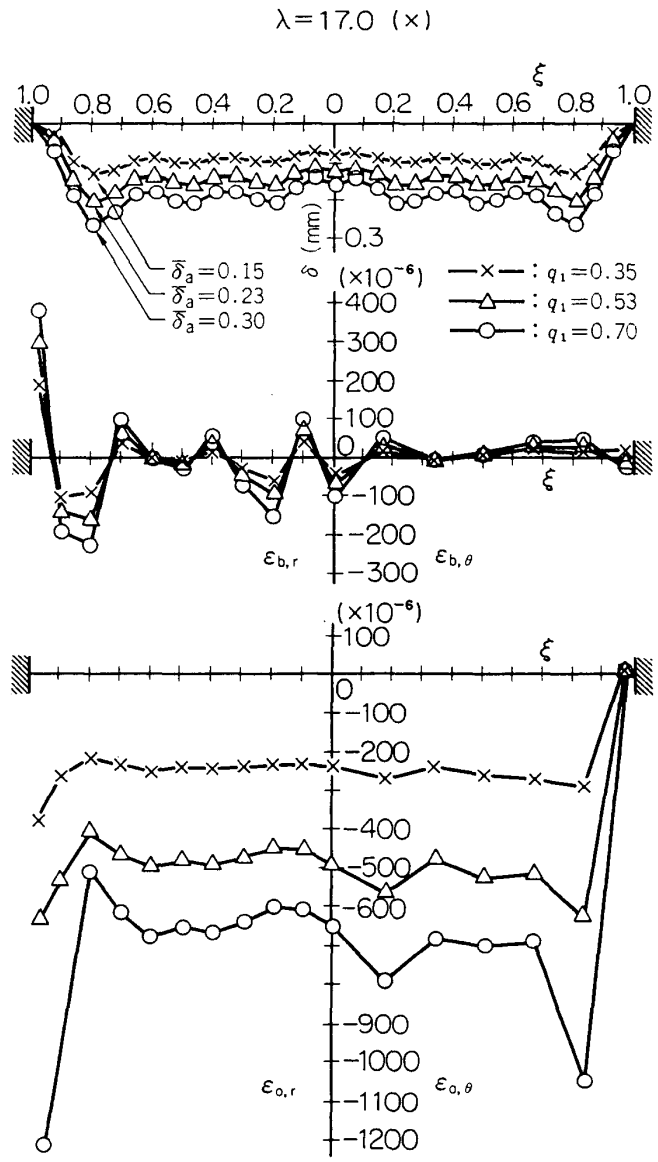

FIG. 19 (t)

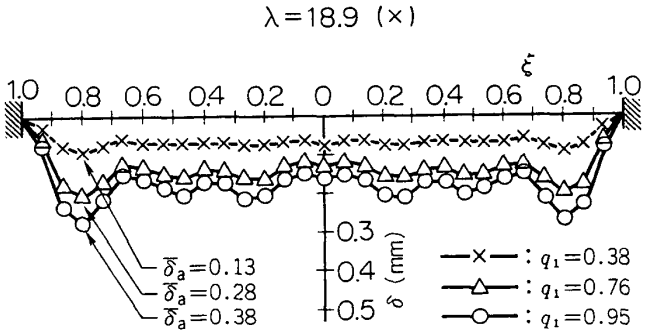

FIG. 19 (u)

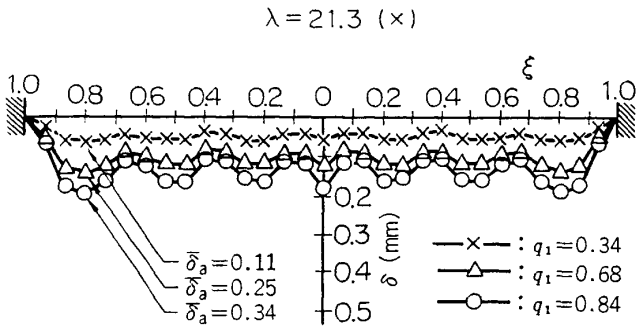

FIG. 19 (v)

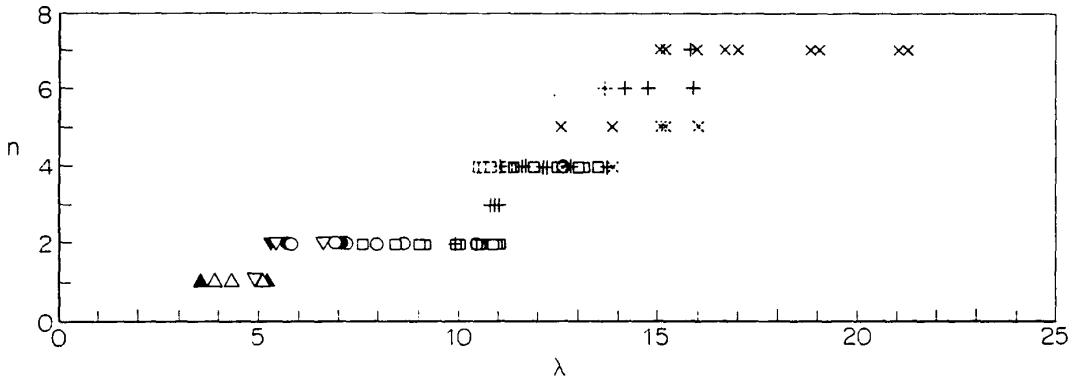

FIG. 20. Predominant meridional wave number.

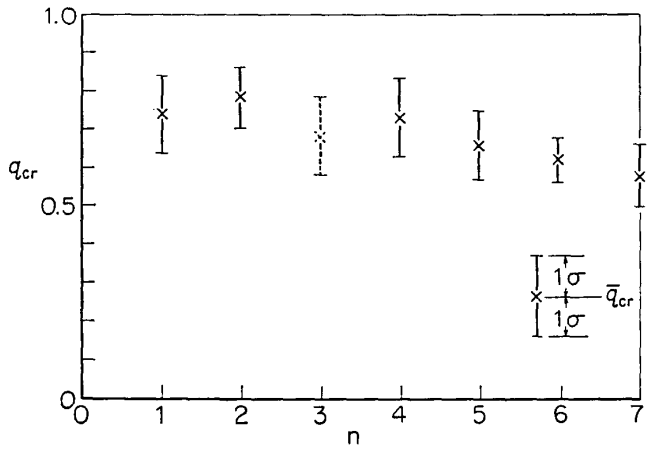

FIG. 21. Variation of q_{cr} with n.

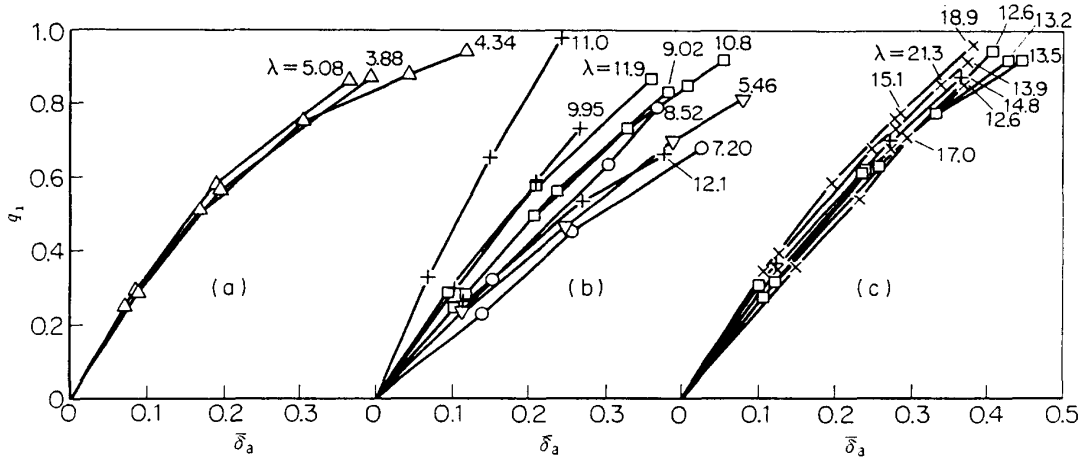

FIG. 22. Relationship between q_1 and $\bar{\delta}_a$.

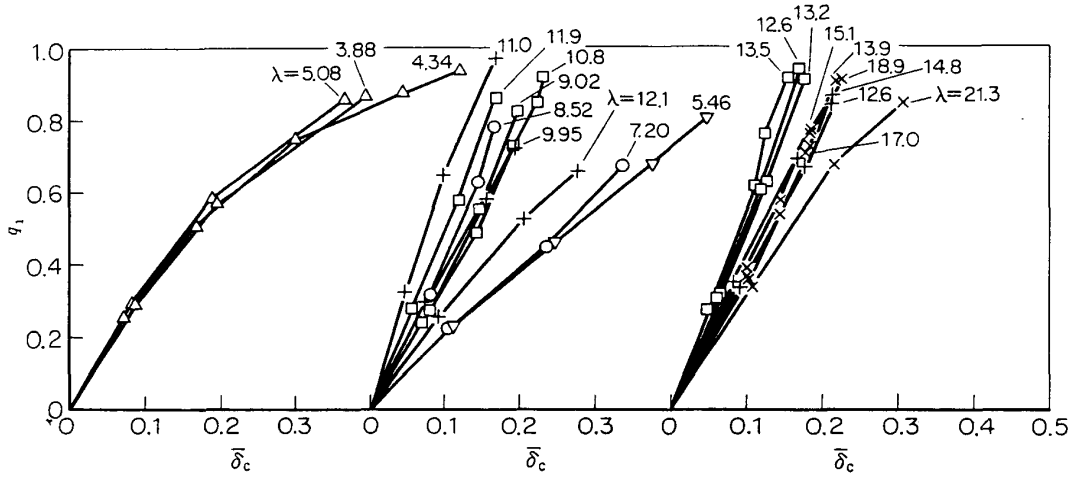

FIG. 23. Relationship between q_1 and $\bar{\delta}_c$.

attribute to the apparatus used. In these measurements, the capacity under specimens was small and the sudden increase of deflection (buckling) of the shell affected the inner negative pressure. It is evident from these figures that the pre-buckling deflection is small especially for cases of larger gometrical parameter and that the relationship between the load and deflection becomes almost linear as the value of geometrical parameter increases.

When values of n increase, the deflection becomes smaller and rippled waves are superimposed on a swell, and hence the precise measurement of deflection by mechanical devices is rather difficult and a wrong selection of locations of transducers results in a incorrect account of wave numbers.

The magnitudes of strains shown in figures are corrected ones taking the effects of curvatures of measured points and local reinforcement by gauges [9] into consideration.

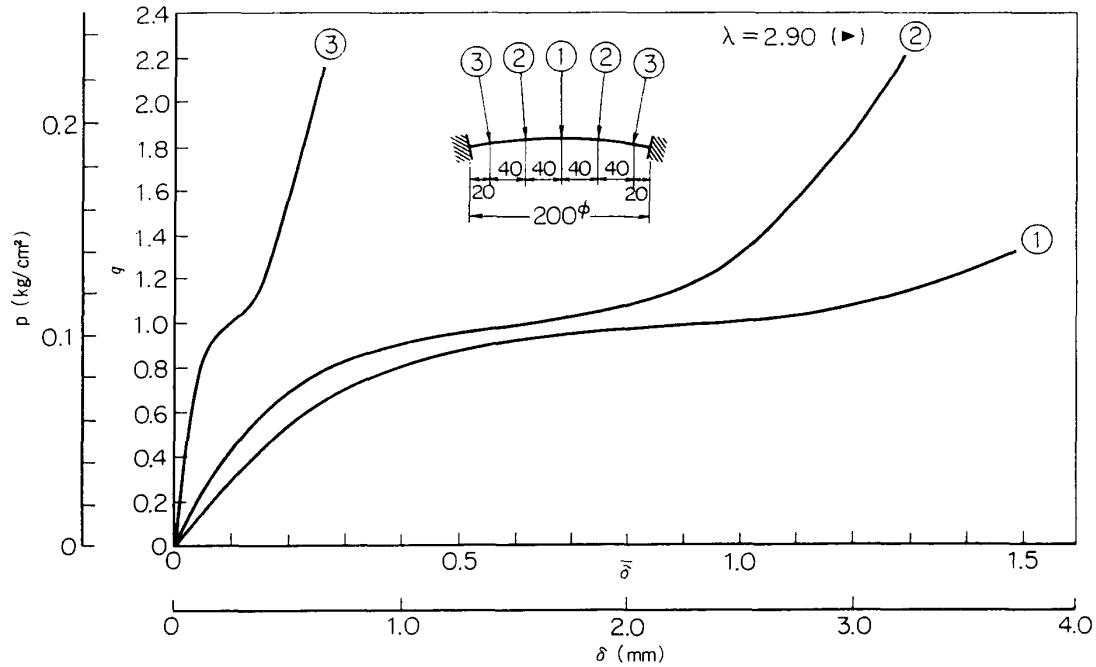

FIG. 24. (a) Relationship between load and displacement.

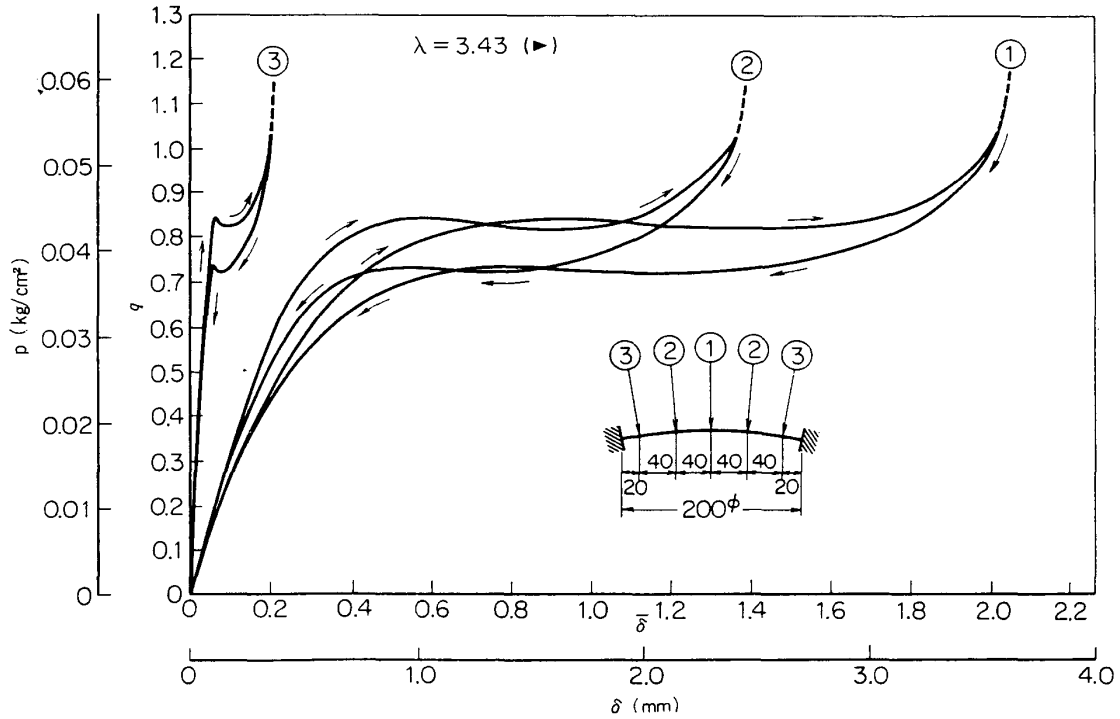

FIG. 24 (b)

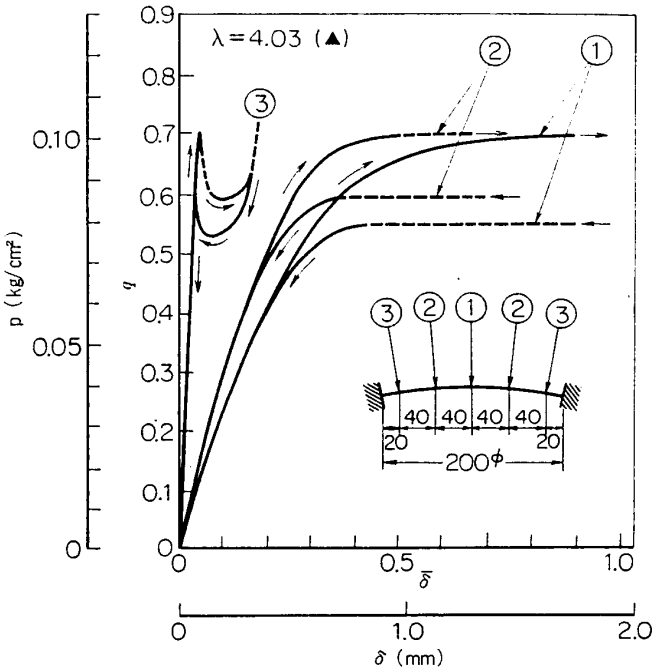

FIG. 24 (c)

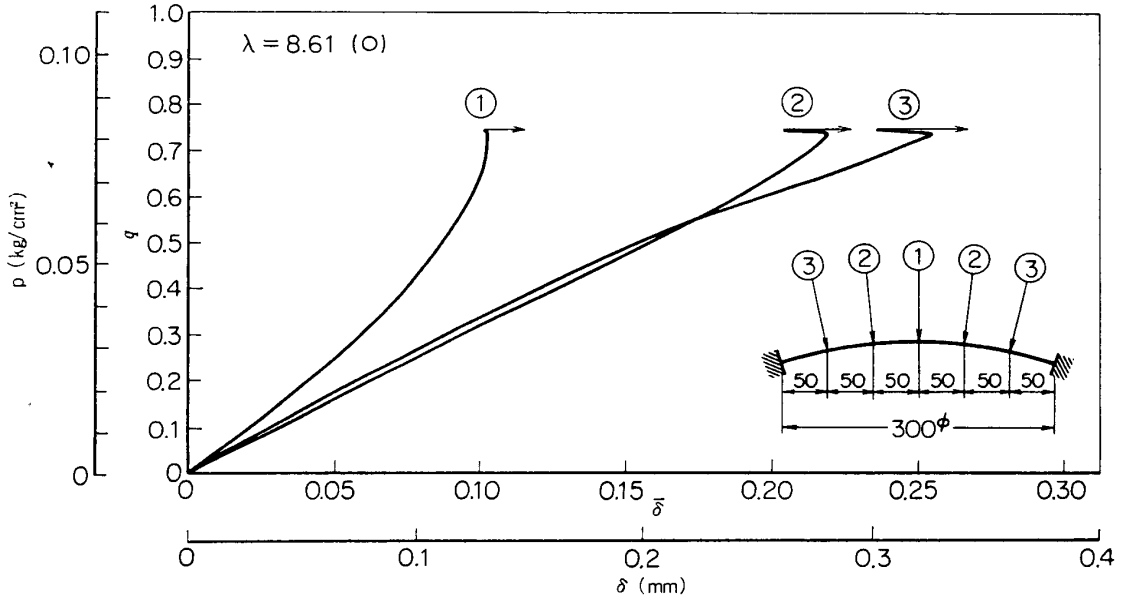

FIG. 24 (d)

4.3. *Buckled Deformation Pattern*

All stable equilibrium configurations after buckling were observed to be the lowest fundamental axisymmetrical patterns ($n=1$).

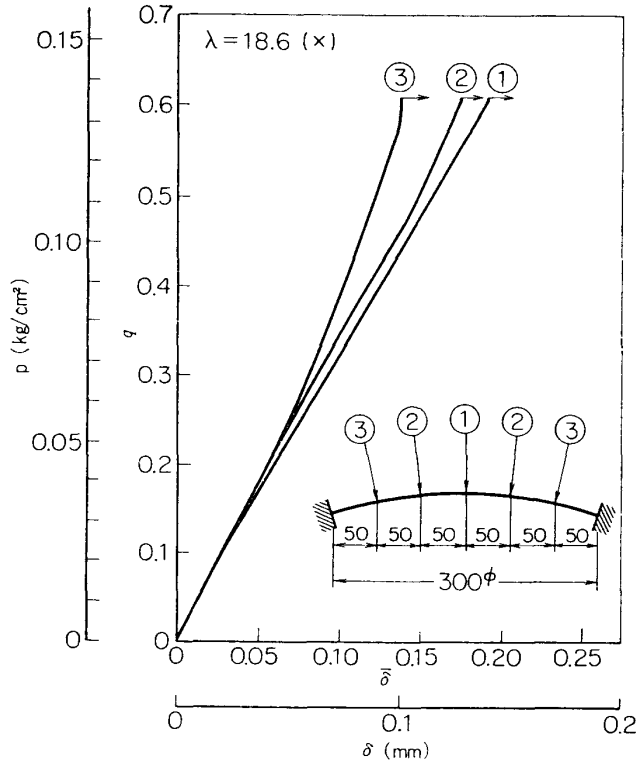

FIG. 24 (e)

5. CONCLUDING REMARKS

In the present paper, on the buckling of spherical caps subjected to external pressure loading the reliable data obtained by a high precision experiment have been reported.

Some remarks and comments given by the authors are summarized in the following:

(1) The buckling load is very close to the classical buckling pressure for the complete spherical shell.

(2) The buckling load is nearly constant up to $\lambda \fallingdotseq 13$ ($\phi \fallingdotseq 50$) and thereafter decreases.

(3) There exists no minimal point around $\lambda=4$ in the buckling load vs. geometrical parameter curve.

(4) No unstable phenomena have been observed for $\lambda<3.25$ ($\phi<3.3$).

(5) It seems that the semi-apex angle has some influence on the buckling load, but the shell thickness and ratio of radius of curvature to thickness do not.

(6) Prebuckling deformation patterns of perfect shells have to be axisymmetrical.

(7) Stable equilibrium configurations after buckling are the lowest axisymmetrical ones.

(8) The deflection is small up to the occurrence of buckling, and when the

geometrical parameter becomes larger the relationship between the load and deflection becomes almost linear.

(9) The in-plane strain increases with the loading, and is generally much larger than the bending strain. It may be one of reasons that buckling loads observed are very close to the classical one for the complete sphere.

(10) Prebuckling deformation patterns are subject to the semi-apex angle, and they are not fixed but change through the loading.

(11) The number of deflection waves in the meridional direction changes through the loading, and it increases as the value of geometrical parameter increases.

(12) The shell becomes very shallow as the value of geometrical parameter decreases. And the existence of a slight imperfection makes the behavior of shells something like that of a non-flat plate subjected to a transverse loading. This might give a reason why experimental buckling loads have scattered for cases of smaller values of geometrical parameter.

(13) For cases where the geometrical parameter is large, the so-called boundary layer is generated. It seems that this phenomena give an important effect on the buckling load. That is, there exist relatively small axisymmetrical rippled waves outside the boundary layer and this state might be stable in the small but unstable in the large. An analysis on the dynamic response of shallow spherical shells by one of the authors [*18*] has shown that the energy transfer between deformation modes plays an important role in the stability and shells buckle finally into the lowest mode. It can be considered, in practical cases, that the larger the geometrical parameter is, the more tendency to fall into unstable state will exist due to the triggering effects including that of imperfections. In fact, the buckling load becomes smaller as the value of geometrical parameter increases. The fact mentioned above might give some insight into the mechanism of practical occurrence of buckling.

(14) It may be reasonable to consider that the linear theory plays still an important role in analyzing the behavior of spherical caps subjected to external pressure.

Many observations of the snapping behavior of shells in which the authors greatly interested have also been carried out by the use of a high speed movie camera. The photo-elastic analysis of the behavior has also been developed using test specimens made of photo-elastic materials. The detailed accounts on these developments will be published separately.

Department of Structures,
Institute of Space and Aeronautical Science,
The University of Tokyo.
January 1, 1974.

REFERENCES

[*1*] Sunakawa, M.: Recent Trends of the Research on the Buckling of Spherical Shells (A Critical Survey), Jour. Japan Soc. Aeron. Space Sci., **16** (1968), 236.

[*2*] Budiansky, B.: Buckling of Clamped Shallow Spherical Shells, Proc. of the Symposium on the Tehory of Thin Elastic Shells, IUTAM, Delft, Holland, 1959, (1960), 64.

[*3*] Huang, N. C.: Unsymmetrical Buckling of Thin Shallow Spherical Shells, Jour. Appl. Mech., **31** (1964), 447.

[*4*] Kaplan, A. and Fung, Y.-C.: A Non-Linear Theory of Bending and Buckling of Thin Elastic Shallow Spherical Shells, NACA TN 3212, (1964).

[*5*] Homewood, R. H., Brine, A. C., and Johnson, A. E., Jr.: Experiental Investigation of the Buckling Instability of Monocoque Shells, Exptl. Mech., **1** (1961), 88.

[*6*] Krenzke, M. A. and Kiernan, T. J.: Elastic Stability of Near-Perfect Shallow Spherical Shells, AIAA J., **1** (1963), 2855; erratum **2** (1964), 784.

[*7*] Sunakawa, M. and Ichida, K.: Buckling of Spherical Shells Subjected to External Pressure, 1st Report, Jour. Japan Soc. Aeron. Space Sci., **21** (1973), 263.

[*8*] Sunakawa, M. and Ichida, K.: ibid. 2nd Report, ibid., **21** (1973), 384.

[*9*] Sunakawa, M., Ichida, K., and Sunaga, Y.: Annual Meeting, Tōkai Branch, Japan Soc. Mech. Eng., Nagoya, March 19, 1968.

[*10*] Sunakawa, M., Ichida, K., and Sunaga, Y.: 10th Structures and Structural Dynamics Conference, Japan Soc. Aeron. Space Sci. and Japan Soc. Mech. Eng., Nagoya, July 6, 1968.

[*11*] Sunakawa, M., Ichida K., and Sunaga, Y.: 12th Internat. Congr. Appl. Mech., IUTAM, Stanford, August 26–31, 1968.

[*12*] Sunakawa, M. and Ichida, K.: 18th Japan Nat. Congr. Appl. Mech., Tokyo, November 8–9, 1968.

[*13*] Sunakawa, M. and Ichida, K.: Annual Meeting, Japan Soc. Aeron. Space Sci., Tokyo, April 5–7, 1971.

[*14*] Sunakawa, M. and Ichida, K.: 14th Structures and Structural Dynamics Conference, Japan Soc. Aeron. Space Sci. and Japan Soc. Mech. Eng., Fukuoka, July 12–14, 1972.

[*15*] Sunakawa, M.: A Note on the Stability of Shells (An Invited Paper), 22nd Japan Nat. Congr. Appl. Mech., Tokyo, December 5–6, 1972.

[*16*] Ichida, K., Kumai, N., and Sunakawa, M.: A Comment on Gauge Factor of Wire-Resistant Strain Gauges, Jour. Japan Soc. Aeron. Space Sci., **20** (1972), 16.

[*17*] Kumai, N. and Sunakawa, M.: Dynamic Response of Viscoelastic Shallow Spherical Shells, Inst. Space Aeron. Sci., The University of Tokyo, Bulletin, 8–2 (B) (1972), 355.

[*18*] Kumai, N. and Sunakawa, M.: Response of Viscoelastic Shallow Spherical Shells to Dynamic Pressures, Jour. Japan Soc. Aeron. Space Sci., **19** (1971), 452.